Iranian Journal of Basic Medical Sciences
ijbms.mums.ac.ir

Evaluation of differentiation of the umbilical cord blood-derived mesenchymal stem cells into male germ-line cells in two-dimensional and three-dimensional scaffolds containing naringin

Arian Azimi [1], Arian Ehterami [2], Sepehr Zamani [3], Seyede Nazanin Aghayan[3], Seyed Meysam Yekesadat [4], Fariborz Sharifianjazi[5], Sina Sohrabi[6], Morteza Alizadeh[7], Majid Salehi [8, 9]*

[1] Department of Anatomical Sciences, Tarbiat Modarres University, Tehran, Iran
[2] Institute for Regenerative Medicine (IREM), University of Zurich, Zurich, Switzerland
[3] Student Research Committee, School of Medicine, Shahroud University of Medical Sciences, Shahroud, Iran
[4] Clinical Research Development Unit, Imam Hossein Hospital, Shahroud University of Medical Sciences, Shahroud, Iran
[5] Center for Advanced Materials and Structures, School of Science and Technology, the University of Georgia, Tbilisi 0171, Georgia
[6] Student Research Committee, School of Dentistry, Golestan University of Medical Sciences, Gorgan, Iran
[7] Department of Tissue Engineering and Biomaterials, School of Advanced Medical Sciences and Technologies, Hamadan University of Medical Sciences, Hamadan, Iran
[8] Regenerative Medicine Research Center, Shahroud University of Medical Sciences, Shahroud, Iran
[9] Department of Tissue Engineering, School of Medicine, Shahroud University of Medical Sciences, Shahroud, Iran

ARTICLE INFO

Article type:
Original

Article history:
Received: Jun 15, 2025
Accepted: Oct 25, 2025

Keywords:
Biocompatible materials
Freeze drying
Germ cells
Mesenchymal stem cells
Nanofibers

ABSTRACT

Objective(s): This study aimed to investigate the differentiation potential of human umbilical cord blood-derived mesenchymal stem cells (UCB-MSCs) into male germ-like cells using a three-dimensional poly (L-lactic acid)/gelatin nanofiber (PLLA/GNF) scaffold incorporated with naringin (Nar).

Materials and Methods: The composite scaffold was fabricated by freeze-drying a PLLA solution containing 1% Nar and electrospun GNFs. Scaffold characterization included morphological analysis, porosity assessment, drug release profiling, and biodegradation testing. UCB-MSCs were isolated and characterized for surface markers ($CD44^+/CD90^+/CD34^-/CD45^-$) via flow cytometry. Cells were seeded onto scaffolds and differentiated using BMP4 (25 ng/ml) alone or in combination with retinoic acid (10^{-6} M). Evaluations included the MTT assay for viability, immunofluorescence for germ cell markers (PLZF, DAZL, OCT4), and *in vivo* biocompatibility assessed by subcutaneous implantation in rat models.

Results: The scaffold demonstrated optimal physical properties, with a porosity of 81.13 ± 2.22% and an average pore size of 108.31 ± 9.29 µm. Nar release profile showed sustained delivery with cumulative release of 38.5 ± 5.72% over 14 days. Biodegradation rate reached 51.07 ± 5.64% after 14 days. MTT assay revealed significantly enhanced cell proliferation in Nar-containing scaffolds at both 24 and 72 hr ($P< 0.05$). Immunofluorescence analysis demonstrated markedly higher expression of germ cell markers in 3D cultures compared to 2D controls. In vivo evaluation confirmed excellent biocompatibility with minimal inflammatory response.

Conclusion: The 3D PLLA/GNF/Nar scaffold creates a favorable microenvironment that effectively promotes UCB-MSC differentiation into male germ-like cells, representing a promising platform for reproductive tissue engineering applications.

▶ Please cite this article as:
Azimi A, Ehterami A, Zamani S, Aghayan SN, Yekesadat SM, Sharifianjazi F, Sohrabi S, Alizadeh M, Salehi M. Evaluation of differentiation of the umbilical cord blood-derived mesenchymal stem cells into male germ-line cells in two-dimensional and three-dimensional scaffolds containing naringin. Iran J Basic Med Sci 2026; 29:

Introduction

The World Health Organization (WHO) defines infertility as the inability of couples of reproductive age to conceive after one year of unprotected sexual intercourse. The 2005 National Survey of Family Growth indicates that this disease affects roughly 13-15% of couples worldwide (1). A primary factor contributing to this discrepancy is the unequal distribution of resources dedicated to the diagnosis and treatment of infertility. Consequently, there is a pressing need for innovative approaches to address this issue.

Mesenchymal stem cells (MSCs) possess unique capabilities for multipotent differentiation and are typically classified by source, including embryonic and adult stem cells. Prior research has identified bone marrow, adipose tissue, skin tissue, and synovial membrane as the principal sources for harvesting adult stem cells (2). Additionally,

***Corresponding author:** Majid Salehi. Regenerative Medicine Research Center, Shahroud University of Medical Sciences, Shahroud, Iran, Department of Tissue Engineering, School of Medicine, Shahroud University of Medical Sciences, Shahroud, Iran.Email: msalehi.te1392@gmail.com

extra-embryonic tissues such as the placenta, amniotic membrane and fluid, and umbilical cord matrix can serve as sources for the collection of mesenchymal stem cells (MSCs) (3, 4). Furthermore, the commonly employed method for this objective is advantageous because it is noninvasive, poses no ethical concerns, and does not elicit an immune response in the host animals (5).

Umbilical cord blood (UCB) transplantation has been utilized in clinical practice for many years (6). Furthermore, various studies have demonstrated that multipotent MSCs derived from the umbilical cord (UC) possess a significant capacity for multilineage differentiation, including differentiation into bone, adipocytes, and osteoblasts, among others (7-9). Conversely, prior research has demonstrated that Embryonic Stem Cells (ESCs) can differentiate into the germ cell lineage (10, 11). Furthermore, recent research has demonstrated that primordial germ cell (PGC) and sperm-like cell development occur following ESC differentiation. Notably, one study reported the successful generation of mature, functional sperm from mouse ESCs that produced viable offspring (12-14).

Scaffolds are widely used to enhance interactions between nanoscale surfaces and cellular receptors. A prominent technique employed in scaffold fabrication is electrospinning, which produces scaffolds characterized by high porosity, a diverse pore-size distribution, ultrafine continuous fibers, and a high surface-to-volume ratio. These attributes can simulate the natural extracellular matrix (ECM) of specific tissues (15). Different materials are used for fabricating electrospun scaffolds. Still, among them, naturally-derived polymers and synthetic-based polymers are used more than others because of their appropriate properties, such as biodegradability, biocompatibility, etc (16). Freeze-drying, also known as lyophilization, is a widely employed method for the production of bioactive scaffolds characterized by a porous architecture with three-dimensional geometries (17). The process comprises four phases: pretreatment or formulation, freezing, primary drying, and secondary drying (18). Using this method enables the creation of a high-porosity scaffold characterized by interconnected pores of appropriate size. In contrast, the scaffold's aligned structure enhances its mechanical properties without altering its composition (19, 20).

Gelatin is a commercially available biopolymer that has appropriate biocompatibility, non-immunogenicity, and biodegradability (21, 22). The mechanical properties of gelatin scaffolds are inadequate; to address this issue, these scaffolds are typically combined with other polymers (23). Poly (L-lactic acid) (PLLA) has good mechanical properties and is used in different parts of tissue engineering (24, 25). Moreover, previous studies indicated that PLLA scaffolds enhance the *in vitro* aggregation of spermatogonial cells sourced from newborn male mice, promoting their differentiation throughout cultivation (26).

Naringin (Nar) (4', 5, 7-trihydroxyflavanone 7-rhamnoglucoside) is a flavanone glycoside obtained from grapefruit, tomatoes, and many citrus fruits. This chemical demonstrates a variety of advantageous features, including anti-inflammatory, anti-apoptotic, anti-osteoporotic, anti-carcinogenic, anti-ulcer, and particularly, neuroprotective benefits (27-29). Therefore, it is widely used for bone regeneration, cancer therapy, treatment of central nervous system diseases, etc. Furthermore, the prior research highlighted the significant role of Nar in the differentiation of bone marrow stem cells (30).

This study employs umbilical cord blood-derived mesenchymal stem cells (UCB-MSCs) to examine the influence of a 3D environment and the natural flavonoid Nar on their differentiation into male germ-like cells. While it is established that MSCs can differentiate into germ cells, replicating the complex physiological environment necessary for successful spermatogenesis *in vitro* remains exceedingly challenging. Most previous studies have either utilized exclusively 3D scaffolds or focused on biochemical induction within two-dimensional (2D) cultures. However, their method used only the scaffold's physical structure and didn't add any specific bioactive molecules to support the differentiation process. Conversely, certain studies have employed soluble factors such as growth hormones and retinoic acid in basic cultures, frequently neglecting the critical 3D extracellular matrix support, resulting in inadequate cell maturation and functionality. The lack of understanding underscores the need for a more advanced, integrated approach that integrates the physical characteristics of a 3D scaffold with targeted biochemical stimulation. Additionally, the function of anti-oxidants in mitigating oxidative stress—a recognized impediment to spermatogenesis—within a 3D engineered context remains predominantly unexamined. Fan *et al.* established that Nar can promote the osteogenic differentiation of bone marrow mesenchymal stem cells by regulating particular microRNA pathways (31). However, its prospective application in a three-dimensional context to direct germline differentiation is entirely uncharted territory. The innovative aspect of our study is the creation and use of a composite PLLA/GNF scaffold that not only mimics a 3D structure but also acts as a delivery system for the long-term release of Nar. We hypothesize that this combined method will make the microenvironment more supportive, thereby helping UCB-MSCs survive, grow, and eventually differentiate into male germ-like cells by providing topographical, mechanical, and biochemical signals that are highly similar to those found in the testicular niche *in vivo*. To achieve this, gelatin nanofibers were fabricated via electrospinning and incorporated into a PLLA solution containing 1% Nar. Comprehensive characterization analyses were performed on the prepared scaffold, followed by seeding cultured UCB-MSCs onto it. Finally, a series of assays was conducted to evaluate their differentiation potential toward male germ-like cells.

Materials and Methods

Chemicals

The materials and solvents employed in this experiment were obtained from Sigma-Aldrich (St. Louis, USA) and Merck (Darmstadt, Germany), unless otherwise specified.

Gelatin nanofiber (GNF) fabrication via the electrospinning method

Electrospinning was utilized to manufacture gelatin nanofibers. In short, type B gelatin powder generated from cow's skin was dissolved in a 75% (v/v) aqueous acetic acid solution to create a 40% (w/v) gelatin solution. A 10-ml disposable syringe fitted with an 18-gauge stainless steel needle was filled with the produced solution and then connected to a 20 kV high-voltage power supply (Fanavaran Nano-Meghyas, Tehran, Iran). The solution was given at a continuous flow rate of 0.40 ml/hr using a syringe pump (Fanavaran Nano-Meghyas, Tehran, Iran). An aluminum foil collector was placed 15 cm from the needle tip during

electrospinning. The electrospun mats were exposed to glutaraldehyde vapor (15% in ethanol) for 24 hr following fiber deposition, causing crosslinking. The scaffolds were then mechanically broken up into tiny pieces (GNFs), dried in a nitrogen chamber for the entire night, and carefully cleaned with 100 mM glycine solution.

Preparation of PLLA/GNFs scaffold via freeze-drying technique

Initially, 5% (w/v) PLLA dissolved in 1,4-dioxane was stirred for 24 hr. Then the GNFs were added to the stirring PLLA solution (50% (w/w) of GNFs to PLLA)[Weatherbee, 2021 #97;Weatherbee, 2021 #97]. Afterward, Nar was added to the PLLA/GNF solution at a mass percentage of 1% and stirred at room temperature for 12 hr. The combination was stored at -80 °C for 1 hr and subsequently freeze-dried (Telstar, Terrassa, Spain) for 48 hr.

Characterization of the scaffolds

Scanning electron microscopy (SEM) analysis

A scanning electron microscope (SEM; KYKY Technology Development, Beijing, China) operated at an accelerating voltage of 20 kV was used to investigate the ultrastructural morphology of the GNF and PLLA/GNF/Nar scaffolds. To increase surface conductivity, the samples were sputter-coated with a thin gold layer for 250 sec using a sputter coater (SCD 004, Balzers, Germany) before imaging. Using OriginPro 2024 (OriginLab, Northampton, MA, USA) in conjunction with ImageJ software (National Institutes of Health, Bethesda, MD, USA), the mean pore diameter was measured. To guarantee statistical reliability, pore size measurements were done for every image at 20 randomly chosen sites (32).

Porosity assessment

The porosity level of scaffolds is an essential factor for cell culture. The liquid displacement technique and equation 1 were used to determine the porosity percentage of the fabricated scaffolds (33).

$$Porosity(\%) = \frac{V_1 - V_3}{V_2 - V_3} \times 100 \quad \text{(Eq. 1)}$$

In the above equation, V_1 and V_2 denote the initial volume of 96% ethanol and the volume of ethanol remaining after soaking the scaffold, respectively. V_3 is the volume of ethanol remaining after scaffold removal.

Contact angle measurement

The contact angle measurement device (G10, KRUSS, Germany) was employed to assess the hydrophilicity of the manufactured scaffolds using the sessile drop method. A water droplet was applied to three portions of each sample, and the average angle formed between the droplet and the surface of each sample was determined and recorded (34).

Release of naringin

The samples were incubated in 5 ml of phosphate-buffered saline at 37 °C under static conditions in order to examine the release profile of Nar from the built scaffold. To maintain sink conditions, 500 µl of the supernatant was withdrawn at preset intervals and replaced with an equivalent volume of fresh PBS (35). Using an ultraviolet–visible (UV–Vis) spectrophotometer (λ = 283 nm; Cecil, Cambridge, UK), the quantification of Nar release was carried out in triplicate using the formula (36):

$$\text{Drug Release (\%)} = \left(\frac{\text{The amount of released drug}}{\text{The amount of loaded drug}}\right) \times 100 \quad \text{(Eq. 2)}$$

Degradation rate

The degradation rates of the scaffolds (PLLA/GNF/Nar and PLLA/GNF) were assessed by quantifying mass loss. Following the weighing of three replicates per group, the scaffolds were placed in a tube containing PBS and cultured for 14 days at 37 °C. The samples were extracted from the solution and subsequently dried. Equation 3, in which W_0 denotes the initial weight of the scaffolds and W_1 signifies their dry weight post-removal from the solution, was employed to ascertain the degree of deterioration (37).

Weight Loss (%) = × 100 % (Eq. 3)

Blood compatibility

As an anticoagulant, a 3.8% (w/v) sodium citrate solution was prepared in deionized water. Eight milliliters of rat blood were collected for the hemolysis test, coupled with one milliliter of the anticoagulant, and then diluted with 2.5 mL of normal saline to generate two milliliters of diluted blood. The test sample was a 0.2 ml aliquot of the diluted blood. After 60 min of incubation at 37 °C, the mixture was centrifuged for 10 min at 1500 rpm. A BioTek Synergy 2 Multi-Mode Microplate Reader (BioTek Instruments, USA) was used to measure the absorbance at 545 nm after the supernatant had been carefully moved to a 96-well microplate. The mean absorbance was computed after three measurements were performed. Negative control samples were created by combining 0.2 ml of diluted blood with 10 ml of normal saline, while positive control samples were made by combining 0.2 ml of diluted blood with 10 mlof deionized water. Equation 4 was used to determine the hemolysis %.

Hemolysis% = × 100 % (Eq. 4)

Where Dt is the absorbance of the sample, Dnc is the absorbance of the negative control, and Dpc is the absorbance of the positive control (38).

Cell viability assessment

The MTT assay (3-(4, 5-dimethylthiazol-2-yl)-2, 5-diphenyl-tetrazolium bromide) was used to assess the cytotoxicity of the manufactured scaffolds. In brief, composite scaffolds were sterilized and placed into separate wells of a 96-well plate. After being planted onto the scaffolds, human UCB-MSCs (1×10^4 cells/well) were cultured for one and three days. Fresh DMEM containing MTT solution (0.5 mg/ml) was added to each well after the cells had been washed with PBS. To enable the development of formazan crystals, the plates were incubated for four hours. After removing the supernatant, 150 µl of DMSO was added to dissolve the crystals. An Anthos 2020 microplate reader (Biochrom, Berlin, Germany) was used to detect absorbance at 570 nm after 100 µl aliquots had been gently shaken for 10 min and then moved to a new 96-well plate (39).

Harvest of human umbilical cord blood samples

After obtaining informed consent from each donor, umbilical cord blood samples were collected in accordance with the ethical guidelines established by the Bahar Hospital

Ethics Committee in Tehran, Iran. Venipuncture of the umbilical vein was used to obtain samples from full-term deliveries, and the samples were analyzed within 6 hr of collection. Before being used, the obtained samples were stored in a 100 mM EDTA anticoagulant solution at 22 °C. Gestational age, volume collected, and time spent in storage (from collection to processing) were meticulously recorded for every sample.

Isolation and culture of human UCB-derived MSCs

Mononuclear cells (MNCs) were isolated using a Ficoll-Hypaque density gradient (GE Healthcare) with a density of 1.077 g/ml. Isolated cells were seeded in 25 cm^2 culture flasks at a density ranging from 1×10^7 to 1×10^8 cells/cm^2 using Dulbecco's Modified Eagle Medium–Low Glucose (DMEM-LG; Gibco, Invitrogen) plus 10% fetal bovine serum (FBS; Gibco, Invitrogen), 25 µg/ml amphotericin B, 1% streptomycin sulfate (10,000 µg/ml), 1% L-glutamine (200 mM), and 1% antibiotic–antimycotic solution (10,000 U/ml sodium penicillin). The cultures were maintained at 37 °C in a humidified atmosphere with 5% CO_2. After 48 hr, non-adherent cells were removed, and adherent umbilical cord blood-derived mesenchymal stem cells were cultivated with medium changes every two days. Cells were passaged once they reached 80–90% confluence, and the experiments were conducted using cells from the fourth passage (40, 41).

Flow cytometry analysis of the UCB-MSCs immunophenotypic marker set

Using flow cytometry, the MSC populations were identified. For surface marker analysis, mouse monoclonal antibodies against human CD_{34}, CD_{45}, CD_{90}, and CD_{44} (all from eBioscience) were utilized. As instructed by the manufacturer, cells were treated with each antibody for an hour at room temperature. Data were collected using an Attune flow cytometer (Applied Biosystems) and analyzed using FlowJo software (Tree Star, USA) (42).

Immunocytochemistry (ICC)

Immunocytochemistry was used to validate the absence of hematopoietic stem cell markers (CD_{34} and CD_{45}) and to ascertain if mesenchymal stem cell markers (CD_{44} and CD_{105}) were expressed in umbilical cord blood-derived cells. Briefly, cells were cultivated on coverslips, fixed for 20 min at room temperature with 4% paraformaldehyde, permeabilized for 20 min with 50% cold methanol, blocked for 30 min with 2% bovine serum albumin (BSA), and then incubated for 60 min with primary antibodies against CD_{44} and CD_{105} (1:100 dilution in 0.5% BSA). Cells were rinsed with PBS 3 times before being treated for an hour with FITC-conjugated secondary antibodies (1:100 dilution). Following DAPI (10 µg/ml; Molecular Probes, Eugene, OR, USA) nuclear counterstaining, the samples were mounted on glass slides and examined under a fluorescence microscope (43).

UCB-MSCs differentiation

Osteogenic differentiation

To promote osteogenic development, cells at the fifth passage were subjected to osteogenic media for three weeks, with medium replenishment occurring biweekly. The osteogenesis process was evaluated on a weekly basis. After a brief refurbishment every 3–4 days for 21 days, the cells were rinsed in PBS, fixed in 4% paraformaldehyde, and stained with alizarin red (Sigma-Aldrich) to demonstrate calcium deposition. The osteogenic medium is made up of IMDM enhanced with 0.1 µM dexamethasone (Sigma-Aldrich, St Louis, MO), 10 mM β-glycerol phosphate (Sigma-Aldrich), and 0.2 mM ascorbic acid (AsA; Sigma-Aldrich) (44).

Adipogenic differentiation

To promote adipogenic differentiation, fifth-passage cells were cultured for three weeks in an adipogenic medium. The evaluation of adipogenesis was facilitated by weekly monitoring and biweekly medium changes. 0.5 mM 3-isobutyl-1-methylxanthine (IBMX; Sigma-Aldrich), 1 µM hydrocortisone (Sigma-Aldrich), 0.1 mM indomethacin (Sigma-Aldrich), and 10% rabbit serum (Sigma-Aldrich) are added to IMDM to create the adipogenic medium. For 21 days, the cultural media were switched out every three days. To determine whether neutral lipid vacuoles were present in adipocytes, the cells were washed with PBS, fixed in 4% paraformaldehyde, and stained with Oil Red O (Sigma-Aldrich) (45).

Differentiation of the umbilical cord blood-derived mesenchymal stem cells into male germ-like cells in a three-dimensional environment of scaffolds

UCB-MSCs differentiation to male germ cells by BMP_4 treatment onto scaffolds

In the third group, the sterilized scaffolds were positioned in a 96-well plate, where UCB-MSCs at passage four were exposed to DMEM enriched with 10% FBS, 1% penicillin/streptomycin, and BMP_4 (25 ng/ml; Sigma-Aldrich) to facilitate their differentiation into male germ-like cells. These cells were maintained on the scaffolds in BMP4-supplemented medium for 14 days before being collected for subsequent assays.

UCB-MSCs differentiation to male germ-like cells by BMP_4/RA treatment onto the scaffolds

In the fourth group, we administered BMP_4 (25 ng/mL) and RA (10^{-6} M; Sigma-Aldrich) together in DMEM medium supplemented with 10% FBS and 1% Pen/Strep for a total of 14 days. Both factors were maintained throughout the differentiation period to ensure that the induction conditions remained effective. We refreshed the medium every 48 hr to ensure steady exposure to the factors.

Immunofluorescence analysis in a 3D environment

For differentiation examination, scaffolds were subjected to cross-linking for 24 hr in 4% paraformaldehyde, subsequently fixed in paraffin, and prepared for immunohistochemistry. In summary, tissue samples measuring 5 µm in thickness were dewaxed utilizing xylene and then rehydrated through a sequential series of alcohol solutions. The immunostaining process included an overnight incubation of the slides at 4 °C with anti-PLZF antibody (sc-28319; 1:100), anti-DAZL, and anti-OCT_4 antibody (sc-28319; 1:100), followed by a 1-hr incubation at 37 °C with a goat anti-human conjugate that was conjugated with FITC (sc-2005; 1:200) sourced from Santa Cruz Biotechnology, Inc., located in Santa Cruz, CA, USA. Cell nuclei were stained with 10 µg/ml DAPI (Molecular Probes, Eugene, OR, USA). The samples underwent analysis using a fluorescence microscope (IX71 accessories U-RFL-T; Olympus). The protein concentrations of PLZF, DAZL, and OCT_4 were quantified (46).

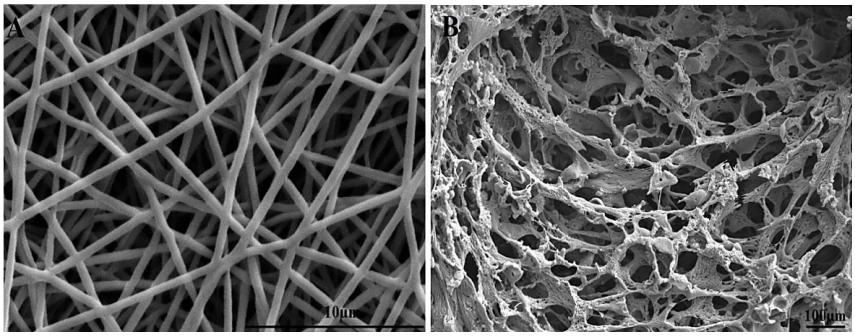

Figure 1. Scanning electron microscopy (SEM) of (A) GNF (Scale bar: 10 µm) and (B) PLLA/GNF/Nar (Scale bar: 100 µm)
Using ImageJ and Origin Pro 2024 software, measured the average fiber diameter of GNFs and the average pore size of the PLLA/GNF/Nar scaffold (n=20 measurements per image). GNF: Gelatin nanofiber, PLLA: Poly (L-lactic acid), and Nar: Naringin

In vivo biocompatibility

To assess the biocompatibility of the synthesized PLLA/GNF/Nar scaffold, a subcutaneous implantation was performed, utilizing a scaffold measuring 1 cm^2, beneath the skin of six male Wistar rats weighing between 200 and 250 g (IR.SHMU.REC.1404.108). The tissue response was closely monitored following the implantation. A histological analysis, employing Masson's trichrome staining, was conducted at two months to evaluate various parameters, including inflammatory responses, foreign body reactions, and vascularization of the scaffold with the adjacent tissue (47, 48).

Statistical analysis

The dataset underwent statistical analysis utilizing SPSS (IBM SPSS Statistics, Version 23, Armonk, New York), applying a one-way ANOVA test, with results expressed as mean ± standard error (SE; n ≥3) (49). A *P*-value of less than 0.05 was considered statistically significant across all evaluations.

Results

Scaffold characterization

Morphologic properties

Figure 1A demonstrates that the fibers within the constructed scaffolds exhibited a random distribution and possessed a consistent, smooth morphology. Statistical analysis revealed an average fiber diameter of 870 ± 45 nm in these scaffolds. Figure 1B depicts the porous architecture of the PLLA/GNFs/Nar scaffold, with the average pore size measured at 108.31 ± 9.29 µm.

Porosity

The porosity of the scaffold structure significantly influences cell migration and implantation. As shown in Table 1, the porosity of the constructed scaffolds was approximately 80% after incorporating Nar.

Biodegradation

We quantified scaffold degradation *in vitro* by measuring the residual mass after immersion in PBS at 37 °C for 7 and 14 days. Table 1 shows that both types of scaffolds lost mass over time, with nearly 50% of the mass lost by the 14th day. There was no statistically significant difference observed between the PLLA/GNF and PLLA/GNF/Nar scaffolds (P>0.05), suggesting that the addition of Nar did not affect the degradation characteristics of the composite structure.

Wettability

The contact angle test can indicate the hydrophilicity of the scaffold surface. The wettability of scaffold surfaces influences cell attachment and their subsequent fate. The hydrophobicity of PLLA/GNF and PLLA/GNF/Nar scaffolds was measured at 84.93 ± 3.76° and 89.24 ± 4.28°, respectively, indicating an increase with the addition of Nar to PLLA/GNF; however, this change was not statistically significant (P>0.05) (Figure 2). Previous studies have shown that Nar has low water solubility, which reduces its availability to the body and complicates studies of its pharmacological effects (50). The hydrophobic nature of Nar caused that when Nar

Table 1. Physicochemical characterization of the PLLA/GNF and PLLA/GNF/Nar scaffolds.
GNF: Gelatin nanofiber, PLLA: Poly (L-lactic acid), and Nar: Naringin

Samples	Porosity (%)	7th Degradation rate (%)	14th Degradation rate (%)
PLLA/GNF	81.13 ± 2.22	39.17 ± 5.36	53.26 ± 4.99
PLLA/GNF/Nar	80.96 ± 2.86	36.88 ± 4.12	51.07 ± 5.64

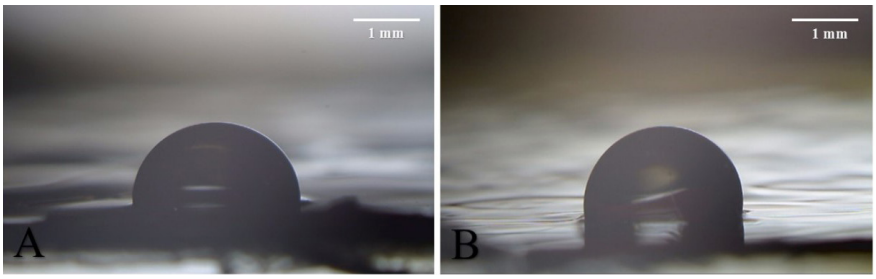

Figure 2. Evaluation of surface wettability by Contact angle measurements of scaffolds: (A) PLLA/GNF and (B) PLLA/GNF/Nar, (Period time: 10 sec, Scale bar: 1mm)
GNF: Gelatin nanofiber, PLLA: Poly (L-lactic acid), and Nar: Naringin

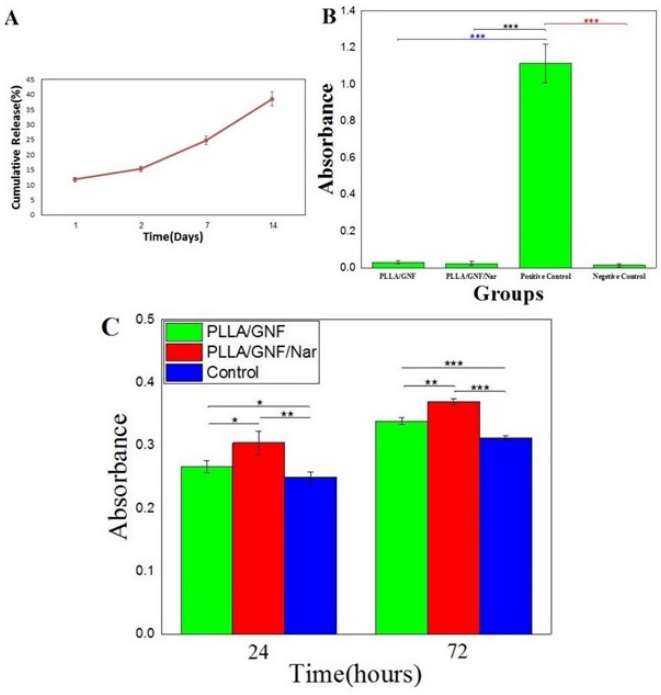

Figure 3. *In vitro* analysis of naringin release, hemocompatibility, and cellular proliferation on the engineered scaffolds
(A) The total amount of Naringin released from the PLLA/GNF scaffold over 14 days, as measured by UV-Vis spectrophotometry at 283 nm. (B) A histogram that shows how well the prepared scaffolds interact with blood cells using a hemolysis test. (C) MTT assay results showing how well UCB-MSCs grew on the different scaffolds after 24 and 72 hr. Values are the mean ± SD (n = 3). **P*<0.05, ***P*<0.01, and ****P*<0.001.

was added to the scaffold, the contact angle increased.

Release

The cumulative release profile of Nar from PLLA/GNFs shown in Figure 3.A. It was proven to release 17.76 ± 2.58% and 15.3 ± 3.43% of released Nar on the first and second days, respectively, and sustained release of 38.5 ± 5.7% for 14 days.

Blood compatibility

Hemolysis resulted in the release of hemoglobin into the plasma as a consequence of erythrocyte destruction, which was directly linked to the compatibility of materials with blood. Figure 3.B illustrates the observed hemolytic levels. The hemolysis levels for all samples were found to be lower than those of the positive control, and these differences were statistically significant.

Cytotoxicity results

The cytotoxicity of the synthesized scaffolds was evaluated utilizing the MTT assay at 24 and 72 hr after cell seeding, with the results depicted in Figure 3.C. The results showed that the scaffolds did not exhibit any cytotoxic effects and instead facilitated cell growth. Figure 3.C illustrates the positive influence of Nar on cell proliferation at both time intervals. Notably, cell proliferation in the PLLA/GNF/Nar group was statistically significant compared with the control and other experimental groups at both 24 and 72 hr post-cell seeding.

The results of in vitro studies

Derived cells

The characteristics of UCB-MSCs in the fourth passage are illustrated in Figure 4. This indicates that the MSCs adhered to the flask were well-developed and exhibited the defining features of MSCs (for instance, elongated spindle shape).

Flow cytometry analysis

Initially, the derived UCB-MSCs were analyzed through the flow cytometry method. Figure 5 illustrates the flow cytometry analysis, indicating that the derived cells exhibited mesenchymal stem cell markers (CD_{44} and CD_{90}) while lacking the expression of hematopoietic cell surface markers (CD_{34} and CD_{45}).

Immunocytochemistry analysis

Figure 6 indicates the results of the ICC test among specific and non-specific markers. The images clearly showed that the derived cells contained numerous mesenchymal stem cells, whereas only a few hematopoietic stem cells were present. These results confirm the results of flow cytometry analysis.

Osteogenic and adipogenic differentiation

To further evaluate the derived cells, their differentiation into osteogenic and adipogenic lineages was assessed. The process of osteogenic differentiation, indicated by Alizarin Red staining, and adipogenic differentiation, demonstrated by Oil Red staining, is illustrated in Figure 7. These findings were obtained by maintaining the derived cells in differentiation media for 21 days, as previously outlined.

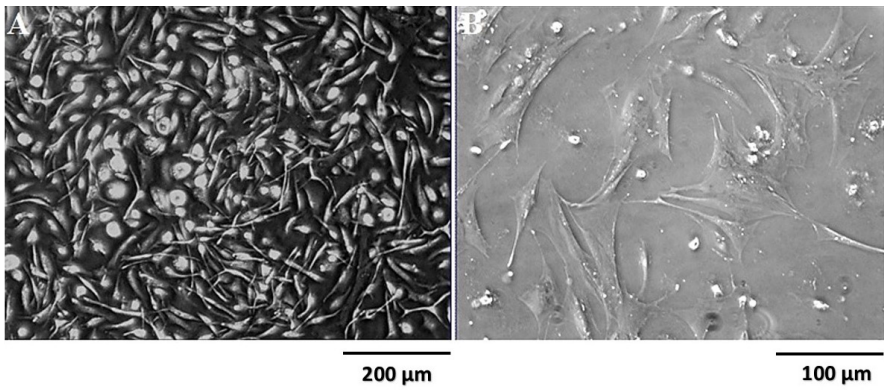

Figure 4. Morphological characteristics of human umbilical cord blood-derived mesenchymal stem cells (UCB-MSCs) at passage 4 prior to differentiation assays. UCB-MSCs exhibited a uniform spindle-shaped morphology and reached approximately 80–90% confluency before being used for downstream differentiation experiments
(A) 200 µm (200x magnification) and (B) 100 µm (400x magnification) are the scale bars. UCB-MSCs: Umbilical cord blood-derived mesenchymal stem cells

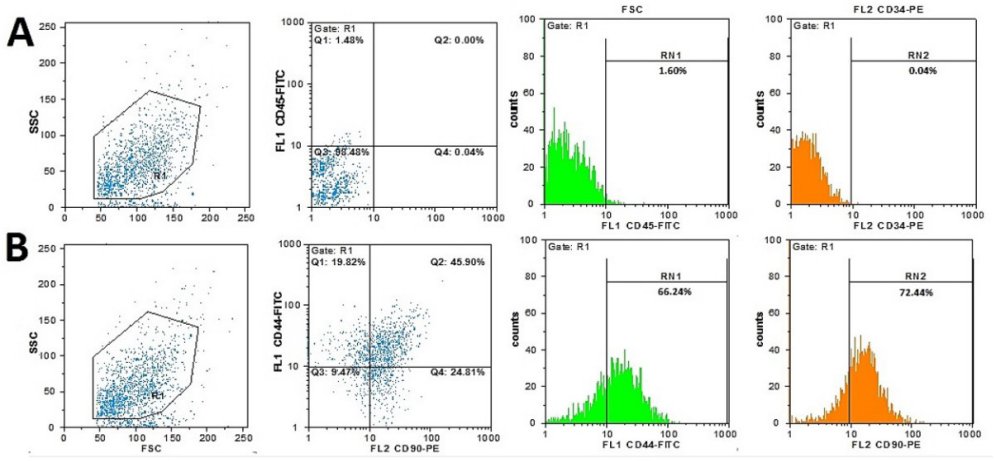

Figure 5. Flow cytometry analysis for the immunophenotypic characterization of derived UCB-MSCs
Histograms illustrate the expression profile of particular cell surface markers on passage 4 UCB-MSCs. (A) Most cells lacked the hematopoietic lineage markers CD34 and CD45 (the filled histogram shows the isotype control). (B) The cells expressed high levels of CD44 and CD90, which are **typical markers** of mesenchymal stem cells. UCB-MSCs: Umbilical cord blood-derived mesenchymal stem cells.

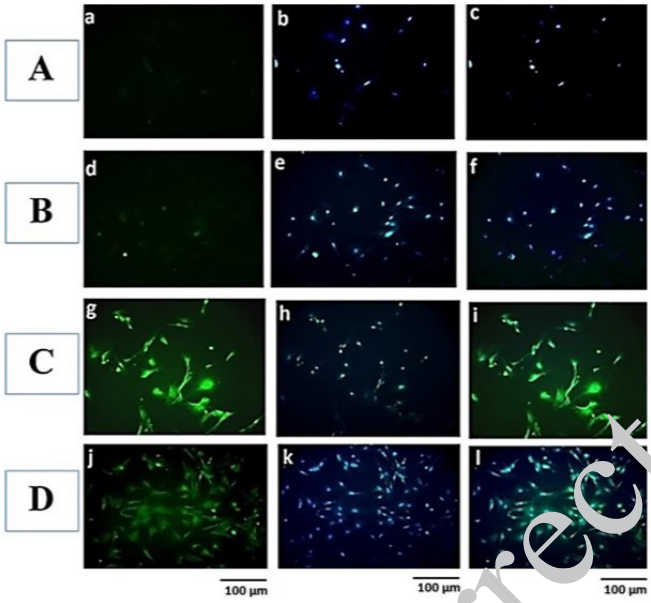

Figure 6. Immunocytochemistry images (200x magnification)
(A) Hematopoietic stem cells a: Primary antibody to CD34 Secondary antibody conjugate with FITC b: Nuclei stain by DAPI c: Merged Fig a & b, (B) Hematopoietic stem cells d: Primary antibody to CD45 Secondary antibody conjugate with FITC e: Nuclei stain by DAPI f: Merged Fig d & e, (C) Mesenchymal stem cells g: Primary antibody to CD44 Secondary antibody conjugate with FITC h: Nuclei stain by DAPI i: Merged Fig g & h, (D) mesenchymal stem cells j: Primary antibody to CD105 Secondary antibody conjugate with FITC k: Nuclei stain by DAPI l: Merged Fig j & k. UCB-MSCs: Umbilical cord blood-derived mesenchymal stem cells, CD: Cluster of differentiation, FITC: Fluorescein isothiocyanate, and DAPI: 4',6-diamidino-2-phenylindole

Immunocytochemistry

To analyze the expression of specific differentiation of UCB-MSCs, PLZF, DAZL, and OCT4 antibodies, 3D groups were used 14 days after starting differentiation, and the results are indicated in Figure 8. As shown in Figure 7, seeded cells differentiated into male germ-like cells across all groups. Moreover, seeded cells were differentiated into male germ-like cells in the 3D environment better than in the 2D environment. In addition, Nar had a positive effect on cell differentiation and improved it in a 3D environment.

In vivo biocompatibility

A histological examination utilizing Masson's trichrome staining was performed at the 2-week post-implantation interval (Figure 9). The observed inflammatory response was minimal and localized, suggesting that the PLLA/GNF/Nar scaffold did not elicit a pronounced acute inflammatory reaction, as evidenced by the absence of immune cells, including macrophages and neutrophils. Furthermore, there was no evidence of a fibrous capsule surrounding the PLLA/GNF/Nar scaffold, which typically signifies a foreign body reaction. Fibroblast activity in the adjacent tissue was moderate, and there were no notable instances of excessive scar formation or granulomatous reactions. The presence of vascularization was clearly observed, characterized by the development of new capillaries within the adjacent skin tissue (White arrow). This observation suggests that the PLLA/GNF/Nar scaffold possesses a notable potential to promote tissue growth and angiogenesis. Finally, mature

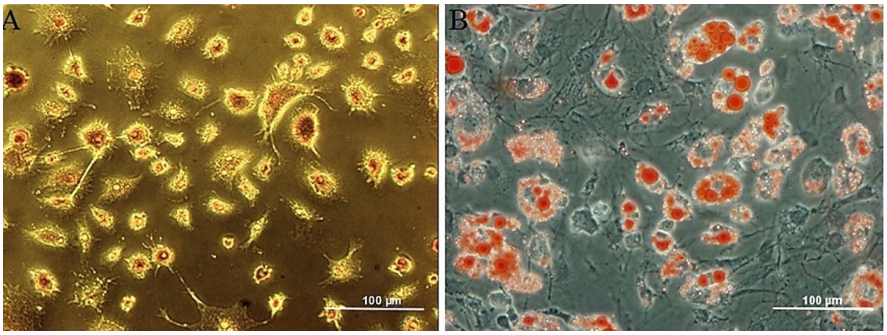

Figure 7. *In vitro* multilineage differentiation potential of UCB-MSCs
(A) Osteogenic differentiation confirmed by Alizarin Red S staining, which detects calcium deposits (red/orange nodules). (B) Adipogenic differentiation confirmed by Oil Red O staining, which highlights intracellular lipid vacuoles (red droplets) within adipocytes. Scale bars: 100 µm (400x magnification). UCB-MSCs: Umbilical cord blood-derived mesenchymal stem cells

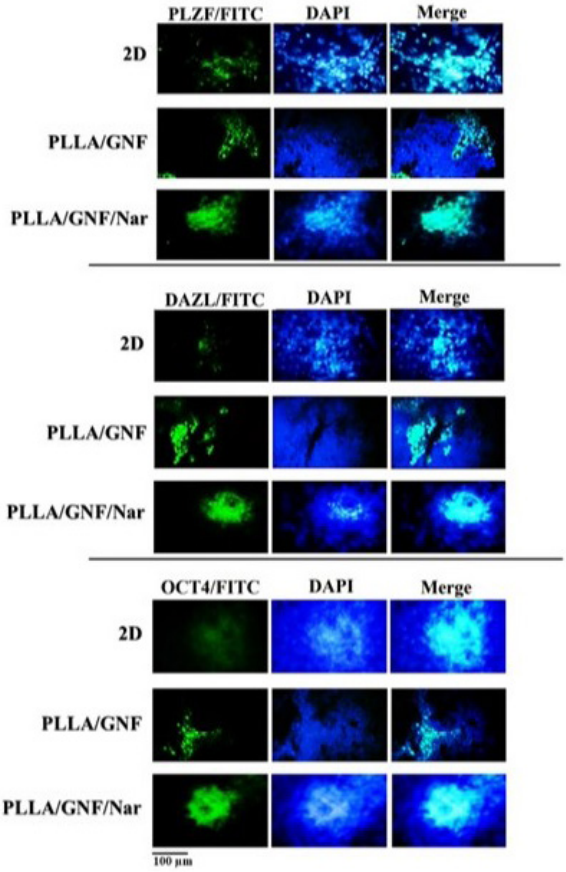

Figure 8. Immunofluorescence analysis of male germ cell-specific marker expression in differentiated UCB-MSCs on 3D scaffolds

Representative fluorescent images of UCB-MSCs cultured for 14 days on PLLA/GNF and PLLA/GNF/Nar scaffolds under different differentiation conditions (BMP4 or BMP4/RA), compared to a 2D culture control. Cells were immunofluorescence-stained for germ cell markers: PLZF (a spermatogonial stem cell marker), DAZL (a meiotic and post-meiotic germ cell marker), and OCT4 (a pluripotency marker also expressed in early germ cells). Nuclei were counterstained with DAPI (blue). The intensity and distribution of positive staining (green) for all markers were significantly enhanced in the 3D culture environments, particularly in the PLLA/GNF/Nar scaffold groups, indicating superior differentiation towards a male germ-like cell lineage. Scale bar: 100 µm (200x magnification). UCB-MSCs: Umbilical cord blood-derived mesenchymal stem cells

collagen fibers (red star) and all skin appendages (sebaceous glands with blue arrows and hair follicles with black arrows) are naturally present in the structure.

Discussion

The researchers were inspired by the expression of markers linked to spermatogenesis by gamete generation to enhance the differentiation process that leads to mature sperm and oocytes. Several studies have indicated this enhancement; for instance, Gilchrist *et al.* investigated *in vitro* oocyte maturation (IVM), but it lacked suitable *in vitro* methods (51). One of the most effective methods to mimic a microenvironment for cell growth and division is tissue engineering, using scaffolds that model natural testicular extracellular matrices. This study investigated the differentiation of mesenchymal stem cells sourced from human umbilical cord blood into male germ-like cells, employing a three-dimensional PLLA/gelatin nanofibrous scaffold infused with Nar. The 3D scaffold loaded with Nar improved the expression of early germ-line markers (such as PLZF, DAZL, and OCT4) and supported cell growth and survival better than traditional two-dimensional culture methods. This indicates that integrating topographical signals with sustained biochemical stimulation may enhance germ-line commitment *in vitro*.

Our results align with prior research demonstrating that PLLA nanofibers establish a conducive microenvironment for spermatogonial stem cells. Eslahi *et al.* showed that PLLA nanofiber scaffolds support the survival and partial differentiation of mouse SSCs after freeze-thaw cycles. They reported this because nanoscale topography and a larger surface area enhance cell-matrix interactions. In our research, we employ a PLLA-based nanofiber structure and enhance the concept by integrating a bioactive component (naringin) to facilitate prolonged signaling (52). Conversely, the biological provenance of collagen-derived gelatin renders this material a compelling option for tissue engineering. PLLA will serve as the foundational structure, whereas gelatin, a protein sourced from natural origins, will offer bioactive sites that facilitate cell adhesion and promote differentiation (53, 54).

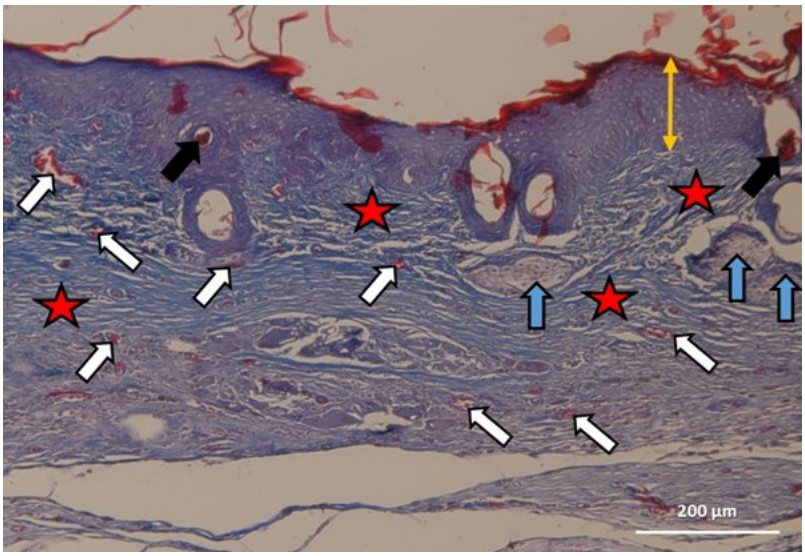

Figure 9. Masson's trichrome staining of subcutaneous implantation of PLLA/GNF/Nar scaffold in Wistar rats after 60 days

Important features include the presence of new blood vessels (white arrow), indicating angiogenesis; mature collagen fibers (red star) in the adjacent dermal tissue; and the normal structure of skin appendages, such as sebaceous glands (blue arrow) and hair follicles (black arrow). These observations collectively demonstrate the scaffold's remarkable biocompatibility and regenerative capacity. Scale bar: 200 µm. GNF: Gelatin nanofiber, PLLA: Poly (L-lactic acid), Nar: Naringin

In a broader context, recent narrative and systematic reviews indicate that three-dimensional systems—such as electrospun fibers, hydrogels, and biomimetic matrices—more effectively maintain the phenotype of spermatogonial stem cells and facilitate differentiation compared to two-dimensional systems, owing to enhanced mass transport and niche-like mechanical properties (55). Additionally, studies show that, in comparison to traditional two-dimensional culture conditions, MSC culture on electrospun nanofiber scaffolds "leads to a reduction in proliferation, a decrease in cellular senescence, and an improved maintenance of stemness (56).

Our results corroborate these reviews and furnish further evidence advocating for the amalgamation of 3D architecture with anti-oxidant and flavonoid delivery. Moreover, data obtained from human-relevant models substantiate the benefits of 3D systems: optimized polycaprolactone and gelatin nanofibers markedly augmented the proliferation of human spermatogonial stem cells relative to control groups, demonstrating that composite, extracellular matrix-mimetic fibers can enhance the preservation and expansion of germ cells—an effect similarly observed with PLLA and gelatin. The translational significance of composite ECM-mimetic fibers for maintaining human germ cells was underscored by Bashiri *et al.*'s consistent reports that, compared with two-dimensional cultures, electrospun PCL/gelatin nanofibrous scaffolds significantly increased proliferation and PLZF expression in human SSCs (57).

Nar has been demonstrated to regulate the Wnt/β-catenin and PI3K/Akt signaling pathways, which are essential for stem cell proliferation and lineage specification. In osteoblast lineage models, Nar enhances β-catenin expression and phosphorylation; it also elevates osteoprotegerin levels through the Wnt/β-catenin pathway in primary fibroblasts, thereby validating the involvement of these pathways in human cells. Although tissue contexts may differ, these conserved pro-survival and pro-differentiation signals likely contribute to the increases in proliferation and germ-line markers observed upon Nar treatment (58, 59).

At the post-transcriptional stage, Nar augments mesenchymal osteogenesis by elevating miR-20a levels and diminishing PPARγ, a regulatory factor that alters MSC fate from adipogenesis to differentiation. In the context of germ-line commitment, directing MSCs toward a pro-differentiation signaling milieu (Wnt/Akt) may enhance their sensitivity to BMP/retinoid signaling, corroborating our results demonstrating enhanced marker induction on scaffolds infused with Nar (60).

Nar also has essential anti-oxidant properties. Oxidative stress makes MSCs less likely to differentiate, but Nar activates Wnt/β-catenin, which encourages osteogenic programs in the presence of ROS. In our study, the 14-day sustained release likely reduced ROS-related apoptosis and preserved sensitivity to morphogens, which explains the enhanced viability and marker expression noted in the Nar groups (61).

Canonical morphogens, BMP4 and retinoic acid, act in concert to initiate germ-line programs. Without BMP4, PGCs can't form. When BMP_4 and RA are combined, they work together to turn on germ-line genes across species and platforms (e.g., iPS-to-male-germ-like differentiation via Smad1/5). Our method, which includes exposing cells to RA/BMP_4 in a three-dimensional, Nar-rich environment, links these biochemical needs to the creation of a physical niche. This is probably why the 3D+naringin setup worked better than the 2D setup (62, 63). Accordingly, Amidi *et al.* showed that human Wharton's jelly-derived MSCs showed an upregulation of several germ-line markers (DDX_4/VASA, DAZL, PLZF) when they were sequentially treated with BMP_4 and RA (or co-cultured with placental feeder cells). This result demonstrates that BMP_4/RA signaling is sufficient to initiate early germ-line gene expression in MSCs derived from umbilical cords (64).

Comparative data demonstrate that there exists a cell-source-specific responsiveness to BMP_4 in the context of germ-like induction, as evidenced by the variations observed between BM-MSCs and AD-MSCs. The use of UCB-MSCs, known for their enhanced proliferative capacity and immunomodulatory effects, may increase BMP4/RA responsiveness within a favorable 3D matrix, thereby supporting our findings relative to prior 2D studies (65).

Electrospun nanofibers mimic (i) fiber diameters akin to those of basement membranes, (ii) anisotropic mechanical properties that promote the alignment of cells and their cytoskeletons, and (iii) a high surface area favorable for protein adsorption, all of which collectively enhance integrin signaling (FAK/Src) and interaction with Wnt/PI3K signaling pathways. Reviews on SSC culture emphasize that three-dimensional constructs—such as alginate hydrogels with Sertoli co-culture, decellularized testicular matrices, and air–liquid interface scaffolds—promote SSC self-renewal and initial differentiation, findings that align with our findings (66).

Some 2D germ-line inductions show only minor improvements in early markers when BMP_4/RA is used alone. Two main reasons could explain our stronger effect: (1) the constant delivery of Nar, which supports pro-survival and pro-differentiation signaling in oxidative environments, and (2) being trapped in a 3D matrix, which improves autocrine/paracrine retention and the creation of local morphogen gradients. The current literature illustrating Nar-induced activation of β-catenin, coupled with reviews emphasizing the distinct benefits of 3D environments, substantiates these claims (67).

We did not fully mature into haploid cells, despite the expression of early germ-line markers being stronger. This exemplifies a prevalent issue in the broader field, where *in vitro* systems often attain a plateau prior to the completion of meiosis. Furthermore, our in vivo assessment of biocompatibility does not evaluate functionality, such as fertilization competence, and the precise dose–response and kinetic mapping for Nar was not comprehensively optimized—both of these factors necessitate further investigation. Investigations using human SSCs in combination with various polymers, including PCL/gelatin, and decellularized matrices suggest that integrating Sertoli cells or testicular extracellular matrix may mitigate these constraints (68).

To improve *in vitro* spermatogenesis, it is best to use Sertoli co-culture or decellularized testicular scaffolds to closely mimic the seminiferous niche, thereby facilitating meiosis. Systematically enhance the release kinetics of Nar by integrating it with GDNF/SCF to promote the self-renewal and development of spermatogonial stem cells. Evaluate genomic stability and functional outcomes, including acrosome formation and ICSI assays, in extended models, employing practical frameworks informed by recent reviews on SSC 3D culture. A 3D PLLA/gelatin

scaffold that offers sustained delivery of Nar improves RA/BMP_4-mediated early germ-line induction from UCB-MSCs by incorporating anti-oxidant protection, pro-differentiation signaling, and niche-mimetic mechanics. This represents a significant advancement over 2D or biochemical-only methods and moves toward functional *in vitro* spermatogenesis.

Conclusion

Our study found that UCB-MSC differentiation into a male germ-like cell was more efficient in the 3D environment than in the 2D environment. Moreover, Nar can enhance differentiation into a male germ-like cell. This research may prove beneficial for *in vitro* examination of spermatogenesis by applying anti-oxidants such as Nar within a 3D PLLA/GNFs scaffold, and for directing stem cell differentiation toward spermatids in the foreseeable future.

Acknowledgment

The present study was supported by Shahroud University of medical sciences. We hereby acknowledge the research deputy for grant No 14040070. In addition, we thank Bahar Hospital, Shahroud, for providing the umbilical cord.

Availability of Data and Material

Not applicable.

Authors' Contributions

A A, A E, SM Y, S S, and SN A designed the experiments, S Z performed experiments and collected data, F SH and M A discussed the results and strategy, M S Supervised, directed and managed the study and final approved of the version. Each author reviewed and endorsed the final manuscript.

Conflicts of Interest

The authors declare that they have no conflicts of interest.

Declaration

The authors thank DeepSeek, a cutting-edge AI platform, for its substantial help in enhancing the language and clarity of this manuscript. We retain full responsibility for the scientific content and ideas, while genuinely appreciating DeepSeek's support in streamlining the editorial process.

References

1.Sullivan EA, Zegers-Hochschild F, Mansour R, Ishihara O, de Mouzon J, Nygren KG, *et al.* International committee for monitoring assisted reproductive technologies (ICMART) world report: Assisted reproductive technology 2004. Hum Reprod 2013;28:1375–1390.
2. Dimarino AM, Caplan AI, Bonfield TL. Mesenchymal stem cells in tissue repair. Front Immunol 2013;4:201-209.
3. Murphy SV, Atala A, eds. Amniotic fluid and placental membranes: Unexpected sources of highly multipotent cells. New York: Thieme; 2013.
4. Batsali AK, Kastrinaki MC, Papadaki HA, Pontikoglou C. Mesenchymal stem cells derived from Wharton's jelly of the umbilical cord: Biological properties and emerging clinical applications. Curr Stem Cell Res Ther 2013;8:144–155.
5. Cequier A, Vázquez FJ, Romero A, Vitoria A, Bernad E, Garcia-Martinez M, *et al.* The immunomodulation–immunogenicity balance of equine mesenchymal stem cells is differentially affected by immune cell response depending on inflammatory licensing and MHC compatibility. Front Vet Sci 2022;9:957153.
6. Wang J, Metheny L. Umbilical cord blood-derived cellular therapy: Advances in clinical development. Front Oncol 2023;13:1167266.
7. Yoo BY, Shin YH, Yoon HH, Seo YK, Song KY, Park JK. Application of mesenchymal stem cells derived from bone marrow and umbilical cord in human hair multiplication. J Dermatol Sci 2010;60:74–83.
8. Xu Y, Meng H, Li C, Hao M, Wang Y, Yu Z, *et al.* Umbilical cord-derived mesenchymal stem cells isolated by a novel explantation technique can differentiate into functional endothelial cells and promote revascularization. Stem Cells Dev 2010;19:1511–1522.
9. Zhang YN, Lie PC, Wei X. Differentiation of mesenchymal stromal cells derived from umbilical cord Wharton's jelly into hepatocyte-like cells. Cytotherapy 2009;11:548–558.
10. Goszczynski D, Navarro M, Mutt A, Ross P. Embryonic stem cells as tools for *in vitro* gamete production in livestock. Anim 2023;17:100828.
11. Odroniec A, Olszewska M, Kurpisz M. Epigenetic markers in embryonal germ cell development and spermatogenesis. Basic Clin Androl 2023;33:6-28.
12. Ishikura Y, Ohta H, Sato T, Murase Y, Yabuta Y, Kojima Y, *et al.* *In vitro* reconstitution of whole male germ-cell development from mouse pluripotent stem cells. Cell Stem Cell 2021;28:2167–2179.
13. Cui YH, Chen W, Wu S, Wan CL, He Z. Generation of male germ cells *in vitro* from stem cells. Asian J Androl 2023;25:13–20.
14. Yang Y, Liu Z, Wu S, Zou L, Cao Y, Xu H, *et al.* Meiosis resumption in human primordial germ cells from induced pluripotent stem cells by *in vitro* activation and reconstruction of ovarian nests. Stem Cell Res Ther. 2022;13:339.
15. Ehterami A, Salehi M, Farzamfar S, Vaez A, Samadian H, Sahrapeyma H, *et al. In vitro* and *in vivo* study of PCL/collagen wound dressing loaded with insulin–chitosan nanoparticles on cutaneous wound healing in rat model. Int J Biol Macromol 2018;117:601-609.
16. Farzamfar S, Naseri-Nosar M, Vaez A, Esmaeilpour F, Ehterami A, Sahrapeyma H, *et al.* Neural tissue regeneration by a gabapentin-loaded cellulose acetate/gelatin wet-electrospun scaffold. Cellulose. 2018;25:1229–1238.
17. Brougham CM, Levingstone TJ, Shen N, Cooney GM, Jockenhoevel S, Flanagan TC, *et al.* Freeze-drying as a novel biofabrication method for achieving controlled microarchitecture within large natural biomaterial scaffolds. Adv Healthc Mater 2017;6:1700598.
18. Fereshteh Z. Freeze-drying technologies for 3D scaffold engineering. In: Functional 3D Tissue Engineering Scaffolds. Amsterdam: Elsevier; 2018. p. 151–174.
19. Fereshteh Z, Fathi M, Bagri A, Boccaccini AR. Preparation and characterization of aligned porous PCL/zein scaffolds as drug-delivery systems via improved unidirectional freeze-drying. Mater Sci Eng C 2016;68:613–622.
20. Ghorbani F, Nojehdehian H, Zamanian A. Physicochemical and mechanical properties of freeze-cast hydroxyapatite–gelatin scaffolds with dexamethasone-loaded PLGA microspheres for hard tissue engineering. Mater Sci Eng C 2016;69:208–220.
21. Samadian H, Salehi M, Farzamfar S, Vaez A, Ehterami A, Sahrapeyma H, *et al. In vitro* and in vivo evaluation of electrospun cellulose acetate/gelatin/hydroxyapatite nanocomposite mats for wound dressing applications. Artif Cells Nanomed Biotechnol 2018;46:964–974.
22. Zamani S, Ehterami A, Vaez A, Naeiji M, Maghsoodifar H, Sadeghi-Douki SAH, *et al.* Natural and synthetic polymers in burn wound healing: A review. J Biomater Sci Polym Ed 2026;37:118-183.
23. Lukin I, Erezuma I, Maeso L, Zarate J, Desimone MF, Al-Tel TH, *et al.* Progress in gelatin as biomaterial for tissue engineering. Pharmaceutics 2022;14:1177-195.
24. Salehi M, Farzamfar S, Bastami F, Tajerian R. Fabrication and characterization of electrospun PLLA/collagen nanofibrous scaffold coated with chitosan to sustain release of aloe vera gel for skin tissue engineering. Biomed Eng Appl Basis Commun

2016;28:1650035.
25. Shahrezaee M, Salehi M, Keshtkari S, Oryan A, Kamali A, Shekarchi B. *In vitro* and *in vivo* investigation of PLA/PCL scaffold coated with metformin-loaded gelatin nanocarriers in regeneration of critical-sized bone defects. Nanomedicine 2018;14:2061–2073.
26. Slahi N, Hadjighassem MR, Joghataei MT, Bakhtiyari M, Ayyoubiyan M, Asadi MH, *et al.* Effects of PLLA nanofiber scaffold on proliferation of frozen-thawed neonatal mouse spermatogonial stem cells. Anat Sci J 2012;9:280–294.
27. Chen R, Qi QL, Wang MT, Li QY. Therapeutic potential of naringin: An overview. Pharm Biol 2016;54:3203–3210.
28. Rong W, Wang J, Liu X, Jiang L, Wei F, Hu X, *et al.* Naringin treatment improves functional recovery by increasing BDNF and VEGF expression after spinal cord injury. Neurochem Res 2012;37:1615–1623.
29. Rong W, Pan YW, Cai X, Song F, Zhao Z, Xiao SH, *et al.* Mechanism of naringin-enhanced remyelination after spinal cord injury. Neural Regen Res 2017;12:470–477.
30. Lin FX, Du SX, Liu DZ, Hu QX, Yu GY, Wu CC, *et al.* Naringin promotes osteogenic differentiation of bone marrow stromal cells via Foxc2 expression through IHH pathway. Am J Transl Res 2016;8:5098-5107.
31. Fan J, Li J, Fan Q. Naringin promotes differentiation of bone marrow stem cells into osteoblasts by regulating microRNA-20a and PPARγ. Mol Med Rep 2015;12:4759–4765.
32. Lam J, Katti P, Biete M, Mungai M, AshShareef S, Neikirk K, *et al.* Universal approach to analyzing transmission electron microscopy with ImageJ. Cells 2021;10:2177-2193.
33. Tayeed MH, Tehranchi M, Ehterami A, Shanei F, Taleghani F, Semyari H, *et al.* Silybin-loaded PCL/gelatin/nanoclay nanocomposite scaffolds enhance bone regeneration: *In vitro* & *in vivo* study. J Biomater Appl 2025;40:105–117.
34. Akbari R, Antonini C. Contact angle measurements: From existing methods to an open-source tool. Adv Colloid Interface Sci 2021;294:102470.
35. Zamani S, Salehi M, Ehterami A, Fauzi MB, Abbaszadeh-Goudarzi G. Curcumin-loaded alginate hydrogel for skin wound healing: gene expression analysis. J Biomater Appl 2024;38:957–9[illegible].
36. Namazi H, Rakhshaei R, Hamishehkar H, Kafil HS. Antibiotic-loaded carboxymethylcellulose/MCM-41 nanocomposite hydrogel films as potential wound dressing. Int J Biol Macromol 2016;85:327–334.
37. Doudi S, Kamalabadi-Farahani M, Atashi A, Amini E, Cheraghali D, Zamani S, *et al.* Injectable multifunctional hydrogel containing sphingosine-1-phosphate and human acellular amniotic membrane for skin wound healing. Iran J Basic Med Sci 2024;27:1134–1147.
38. Zamani S, Rezaei Kolarijani N, Naeji M, Vaez A, Maghsoodifar H, Sadeghi-Douki SAH, *et al.* Carboxymethyl cellulose/gelatin hydrogel loaded with omega-3 for skin regeneration. J Biomater Appl 2024;39:377–395.
39. Esmaeili S, Rahmati M, Zamani S, Djalilian AR, Arabpour Z, Salehi M. Eggshell membrane powder as natural biomaterial for skin regeneration: separation process comparison. Skin Res Technol 2024;30:e70038.
40. Nguyen LT, Tran NT, Than UTT, Nguyen MQ, Tran AM, Do PTX, *et al.* Optimization of human umbilical cord blood-derived mesenchymal stem cell isolation in serum- and xeno-free conditions. Stem Cell Res Ther 2022;13:15-33.
41. De Schauwer C, Meyer E, Cornillie P, De Vliegher S, Van de Walle GR, Hoogewijs M, *et al.* Isolation and characterization of equine umbilical cord blood mesenchymal stromal cells. Tissue Eng Part C Methods 2011;17:1061–1070.
42. Marie D, Rigaut-Jalabert F, Vaulot D. Improved protocol for flow cytometry analysis of phytoplankton cultures and natural samples. Cytometry A 2014;85:962–968.
43. Renshaw S. Immunohistochemistry and immunocytochemistry. In: Essential Methods in Immunohistochemistry and Immunocytochemistry. Oxford: Wiley-Blackwell; 2017. p. 35–102.
44. Wei X, Peng G, Zheng S, Wu X. Differentiation of umbilical cord mesenchymal stem cells into steroidogenic cells versus bone marrow MSCs. Cell Prolif 2012;45:101–110.
45. Sibov TT, Severino P, Marti L, Pavon L, Oliveira D, Tobo P, *et al.* Mesenchymal stem cells from umbilical cord blood: Isolation parameters and adipogenic differentiation. Cytotechnology 2012;64:511–521.
46. Huang HN, Kuo CW, Hung YL, Yang CH, Hsieh YH, Lin YC, *et al.* High-dynamic-range imaging enhances PD-L1 evaluation for 3D pathology in NSCLC. Sci Rep 2024;14:15176.
47. Shanmugam PST, Sampath T, Jagadeeswaran I. Implantation. In: Biocompatibility Protocols for Medical Devices and Materials. Amsterdam: Elsevier; 2023. p. 83–90.
48. Shanmugam PST, Sampath T, Jagadeeswaran I. Biocompatibility protocols for medical devices and materials. Amsterdam: Elsevier; 2023.
49. Seyedi D, Salehi M, Zamani S, Cheraghali D, Dehghani F, Mehrabi M. Alginate/PVA nanofibrous wound dressings containing dragon's blood improve burn wound healing in animal model. J Biomed Mater Res B Appl Biomater 2025;113:e35553.
50. Scheepens A, Tan K, Paxton JW. Improving oral bioavailability of polyphenols through designed synergies. Genes Nutr 2010;5:75-87.
51. Gilchrist RB, Thompson JG. Oocyte maturation: Emerging concepts and technologies to improve developmental potential *in vitro*. Theriogenology 2007;67:6-15.
52. Eslahi N, Hadjighassem MR, Joghataei MT, Mirzapour T, Bakhtiyari M, Shakeri M, *et al.* Poly-L-lactic acid nanofiber scaffold effect on mouse spermatogonial stem cell culture. Int J Nanomedicine 2013;8:4563-4576.
53. Capuana E, Lopresti F, Ceraulo M, La Carrubba V. Poly-L-lactic acid biomaterials for regenerative medicine: Processing and applications review. Polymers 2022;14:1153-1181.
54. Yaraki MT, Dousti B, Karami-Khorramabadi M, Afkhami H. Chitosan/gelatin biodegradable polymers: Potential applications review. Front Bioeng Biotechnol 2024;12:1397668.
55. Fakhri Bayati L, Naserpour L, Khoshandam M, Jannatifar R, Fazeli H. Advances in 3D culture systems for spermatogonial stem cell preservation and differentiation. Int J Reprod Biomed 2023;21:681–696.
56. Heo SJ, Szczesny SE, Kim DH, Saleh KS, Mauck RL. Electrospun scaffolds maintain MSC stemness, mechano-responsivity, and differentiation potential. J Orthop Res 2018;36:808–815.
57. Bashiri Z, Zahiri M, Allahyari H, Esmaeilzade B. Proliferation of human spermatogonial stem cells on optimized PCL/gelatin nanofibrous scaffolds. Andrologia 2022;54:e14380.
58. Wang D, Ma W, Wang F, Dong J, Wang D, Sun B, *et al.* Naringin stimulates Wnt/β-catenin signaling to improve bone development via AMPK and Akt. Cell Physiol Biochem 2015;36:1563–1576.
59. Yang C, Liu W, Zhang X, Zeng B, Qian Y. Naringin increases osteoprotegerin in fibroblasts via Wnt/β-catenin pathway. J Orthop Surg Res 2020;15:600-606.
60. Fan J, Li J, Fan Q. Naringin promotes bone marrow stem cell differentiation into osteoblasts by microRNA-20a regulation. Mol Med Rep 2015;12:4759–4765.
61. Wang H, Liang J, Wang Y, Zheng J, Liu Y, Zhao Y, *et al.* Naringin restores oxidative stress-impaired osteogenic differentiation via Wnt/β-catenin and PI3K/Akt pathways. Sci Rep 2024;14:14047-14060.
62. Yang S, Yuan Q, Niu M, Hou J, Zhu Z, Sun M, *et al.* BMP4 promotes mouse iPS cell differentiation to male germ cells via Smad1/5, Gata4, Id1 and Id2. Reproduction 2017;153:211–220.
63. Yang Y, Feng Y, Feng X, Liao S, Wang X, Gan H, *et al.* BMP4 cooperates with retinoic acid to induce differentiation markers in mouse spermatogonia. Stem Cells Int 2016;2016:9536192.
64. Amidi F, Hoseini MA, Nia KN, Habibi M, Kajbafzadeh AM, Mazaheri Z, *et al.* Germ-like cell differentiation potential of human Wharton's jelly-derived MSCs in co-culture with placenta cells with BMP4 and retinoic acid. Iran J Basic Med Sci 2015;18:325-333.
65. Shirzeyli MH, Tayyebiazar A, Aliakbari F, Ghasemi F, Eini F, Shirzeyli FH, *et al.* Comparison of BMP4 efficacy on *in vitro*

differentiation of murine adipose and bone marrow MSCs into primordial germ cells. Res Pharm Sci 2022;17:123–133.
66. Diao L, Turek PJ, John CM, Fang F, Reijo Pera RA. Roles of spermatogonial stem cells in spermatogenesis and fertility restoration. Front Endocrinol 2022;13:895528.
67. Guo M, Liu F, Wang W, Liu Z, Zhu Z, Liu Y, *et al.* Retracted: Naringin promotes osteogenic/odontogenic differentiation of dental pulp stem cells via Wnt/β-catenin. Evid Based Complement Alternat Med 2022;2022:4505471.
68. Vlajković S, Čukuranović R, Daković Bjelaković M, Stefanović V. Therapeutic use of spermatogonial stem cells in male infertility: Brief overview. Sci World J 2012;2012:374151.